Vacancy and substitutional impurities in the spin-density wave state of Cr from first principles

R. Soulairol,[1] Chu-Chun Fu,[1] and C. Barreteau[2]

[1]*CEA, DEN, Service de Recherches de Métallurgie Physique, F-91191 Gif-sur-Yvette Cedex, France*

[2]*DSM/IRAMIS/SPCSI, CEA/Saclay, F-91191 Gif-sur-Yvette Cedex, France*

(Received 1 March 2011; revised manuscript received 15 April 2011; published 3 June 2011)

Density functional theory (DFT) calculations are carried out to study magnetic and energetic properties of vacancy, and magnetic and nonmagnetic substitutional impurities (respectively Fe and Cu) in the ground state of bcc Cr, i.e., spin-density wave (SDW). We find the lowest energy site for all the defects to be around a magnetic node, as compared with the high-spin SDW sites and (100)-layered antiferromagnetic (AF) and nonmagnetic (NM) phases. The corresponding differences for vacancy formation energy are 0.29, 0.32, and 0.23 eV, respectively. The migration of a vacancy is revealed to be highly anisotropic in the SDW state, mainly confined in the nodal and adjacent planes. The energy barrier for such a quasi-bidimensional motion is indeed 0.52 eV lower than that for migration in perpendicular directions. Regarding magnetic modifications of the SDW introduced by point defects, they are confirmed to be weak and rather local at low defect concentrations (0.27% and 0.55%). Cu behaves similarly to a vacancy-inducing magnetic moment enhancement on neighboring Cr atoms. On the other side, the presence of Fe atoms leads to multiple energy minima with different local magnetic arrangements, particularly around a node, due to competition between neighboring Fe-Cr, Cr-Cr, and Fe-Fe magnetic coupling tendencies. The present results strongly suggest that simple AF and NM phases may not allow an accurate description of defect properties in the ground state of Cr. Instead, an explicit SDW representation is required. In addition, we point out that the presence of vacancy and both Cu and Fe may promote a migration of SDW nodes, which may activate the SDW-to-AF phase transition through a node-annihilation mechanism as proposed in previous works.

DOI: 10.1103/PhysRevB.83.214103 PACS number(s): 71.15.Mb, 71.20.Be, 75.30.Fv, 61.72.J−

I. INTRODUCTION

Although chromium shows a rather simple crystallographic structure in its ground state, i.e., the bcc, it still remains a challenge from a theoretical point of view. This underlying complexity partly comes from its magnetic structure. As observed experimentally, the magnetic ground state of Cr consists of the so-called incommensurate spin-density wave, i.e., an incommensurate long-period modulation of the magnitude of local moments along ⟨100⟩ directions, where nearest-neighbor atoms show antiparallel moments.[1,2] This magnetic arrangement, stable up to the Néel temperature ($T_{\text{Néel}} = 311$ K) in pure Cr, has been proposed to be a direct consequence of the nesting properties of the Cr Fermi surface.[3] It is therefore very sensitive to small modification of the electronic structure. Indeed, first-principles calculations within density functional theory (DFT), despite their satisfactory accuracy in describing other magnetic 3*d* elements, e.g., Fe and Co, all agree in predicting either the antiferromagnetic (AF) or nonmagnetic (NM) state to be the ground state of bcc Cr.[4,5] The experimental magnetic ground state, approximated by a commensurate spin-density wave (SDW) due to periodic-boundary simulations, is a metastable state, a few meV per atom higher in energy than either the AF or the NM state according to DFT. Their relative stability has also been shown to strongly depend on the predicted equilibrium atomic volume.[6–8]

In addition, real materials often contain both structural defects and impurities. To our knowledge, however, most of the previous DFT studies dealing with point defects, e.g., vacancies and self-interstitial atoms in Cr,[9–12] have considered simple AF structures. Such approximation may be supported by the fact that SDWs show large AF domains with high local moments of nearly constant amplitude, connected with smaller regions of low local moments. Note that it could be considered as a satisfactory approximation if the low-moment regions are not relevant to determine properties of defects, which still remains to be verified. Also, the long-range magnetic ordering present in the SDW may influence energetics and mobility of defects. On the other hand, structural defects and impurities may modify the perfect ordering of the SDW state. The effects of 3*d* transition metal (V, Mn, Fe, Co, Ni) and nonmetal (Si) impurities have been investigated experimentally.[13] For instance, a few percent of manganese or vanadium substitutional atoms in Cr are known to modify the periodicity of SDWs by changing electron or hole concentration.[13] A small amount of Fe in Cr has also been suggested experimentally to influence the polarization state of the SDW (longitudinal vs transversal) by decreasing the corresponding spin-flip transition temperature (T_{sf}). The presence of Fe atoms has also been proposed to reduce the temperature stability of the SDW state due to the reduction of $T_{\text{Néel}}$ in Cr. Moreover, it becomes completely unstable against the formation of AF structures with 1.6% of Fe.[13,14] Also, $(\text{Cr} + 1.5\%\,\text{Fe})_{1-x}\text{Mn}_x$ ternary alloys have been proposed to promote the reappearence of the SDW configuration at temperatures between those showing AF and paramagnetic phases for $x = 0.2\%$.[13,15] Very few theoretical studies have been carried out concerning point defects in Cr. For instance, Galkin *et al.* have addressed the specific behavior of Fe in Cr using a phenomenological model based on their magnetic susceptibility measurements.[16] In the case of V, it has been proposed that a threshold concentration of 0.15% was enough to affect the magnetic phase transition in Cr occuring at $T_{\text{Néel}}$.[17] The effects of H insertion at V/Cr interfaces

 ©2011 American Physical Society

have been recently reported by Uzdin *et al.*,[18] showing the destruction of SDWs for an H concentration higher than 50% at the interface layer. On the other hand, a larger amount of studies have been devoted to investigating the stability of the SDW in the presence of extended defects, particularly the Fe/Cr multilayers.[19,20]

Concerning the simplest structural defect, the vacancy (Vac) experiments based on positron annihilation spectroscopy (PAS) provided activation energy for self-diffusion in Cr (Q) for the paramagnetic phase.[21,22] Theoretically, vacancy formation energies in both AF and NM states have been estimated by DFT calculations.[9] But, an accurate prediction of the formation and migration properties of vacancies corresponding to the low-temperature ($T \leqslant T_{\text{Néel}}$) SDW state is still lacking.

In this work, we aim to investigate the properties of vacancies and two representative substitutional impurities by determining in particular, by means of DFT calculations, whether the magnetism of Cr and point defects may influence each other. Section II of this paper describes the calculation methods. The formation and migration of vacancies in the SDW state are presented in Secs. III A and III B, and compared with those in the AF and NM states. Section III C is devoted to addressing the properties and impacts of 3*d* substitutional impurities in the SDW Cr, where Fe and Cu are taken as prototypes of magnetic and nonmagnetic impurities. Section III D details the magnetic and energetic properties of an Fe dimer in Cr. Finally, we compare in Sec. III E different interactions between the point defects (Vac, Fe, Cu) and the SDW structure.

II. METHODOLOGY

The present *ab initio* calculations have been performed within density functional theory as implemented in the SIESTA code.[23] This localized-basis-set DFT approach allows one to deal efficiently with large supercells containing both point defects and complex magnetic structures. Indeed, this approach has been proven in particular to give reliable results about energetics and detailed magnetic structure of SDW in pure Cr,[8] compared with more robust plane-wave codes within the projector-augmented-wave (PAW)[4] and very accurate all-electron approaches.[5] It has also been proven to satisfactorily describe the energetics of point defects in transition metals.[24,25]

The calculations are spin polarized within the collinear approximation. Spin-orbit coupling effects are not included; thus, possible effects of the polarization state of SDW are also neglected. All results are obtained using the generalized gradient approximation (GGA) exchange-correlation functional in the Perdew-Burke-Ernzerhof (PBE) form.

Concerning other DFT approximations, core electrons are replaced by nonlocal norm-conserving pseudopotentials while valence electrons are described by linear combinations of numerical pseudo–atomic orbitals. The pseudopotentials and the basis sets for Cr and Fe atoms are the same as in Ref. 8; those for Cu are the same as in Ref. 26. The accuracy of the Cr, Fe, and Cu pseudopotentials and basis sets has been tested on relevant energetic and magnetic properties, and shown to agree satisfactorily with experimental and plane-wave DFT values.[8,26] The local magnetic moments of the atoms are estimated using the Mulliken criterion.[23]

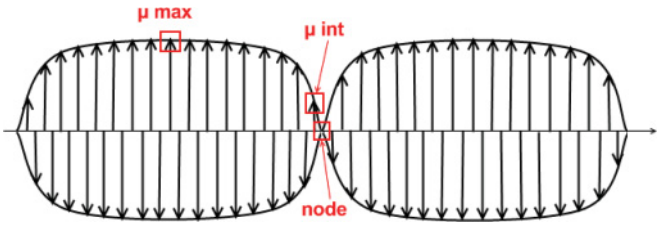

FIG. 1. (Color online) Schematic view of the different sites chosen for point defect in the calculated SDW structure of Cr. Note that μ_{int} and node sites are first-nearest neighbors.

Supercell calculations were performed to study defect properties. Results concerning vacancies and impurities have been obtained adopting $3a_0 \times 3a_0 \times 20a_0$ cells with 360 atoms, a_0 being the lattice parameter of the cubic unit cell. They contain either one period of 9 coherent SDWs along the (001) direction or the same number of Cr atoms in an AF or NM state. The choice of $20a_0$ for the SDW period is to obtain a wave vector $\vec{q}^{\,\text{SDW}} = 0.95$, similar to the low-temperature experimental value.[3] Shifted $4 \times 4 \times 1$ k grids and the Methfessel-Paxton broadening scheme with a 0.3 eV width are used.

We have performed constant-pressure calculations; i.e., the structures are optimized by relaxing both the atomic positions and the shape and volume of the supercell.

To consider point defects in a SDW state of Cr, various inequivalent formation sites need to be considered. In view of the near-sinusoidal shape of SDW,[3,8] we focus our study on 3 representative sites: the node site of zero local magnetic moment, its first neighbor with an intermediate local magnetic moment of 0.5 μ_B in pure Cr (μ_{int} site), and a site of maximum local magnetic moment (1.3 μ_B) in pure Cr (μ_{max} site). They are schematically represented in Fig. 1.

The migration barriers have been calculated at constant volume using the drag method in a fashion similar to that in Refs. 24,25,27: For a given reaction coordinate, the atomic positions relative to the center of mass are constrained to relax within the corresponding hyperplane perpendicular to the vector connecting the initial and final positions.

We have estimated a precision error bar of 0.05 eV for the most relevant energetic values obtained by this study, i.e., the difference between vacancy formation energies (and impurity solution energies) at various magnetic sites, the vacancy migration energies, and the Fe-Fe binding energies in Cr. This error bar accounts for the completeness of the basis sets, the convergence of k-space sampling, and the electronic and the structural relaxations within the present approach. It is worth mentioning that the precision error of such energy differences is generally smaller than that of the formation and solution energies, as systematic errors can be canceled for the former.

III. RESULTS AND DISCUSSION

A. Vacancy formation in SDW Cr

Vacancies are the simplest structural defects, often present in real materials. Physical magnitudes such as their formation and migration enthalpies should be accurately determined in order to gain insight into, e.g., self-diffusion, impurity

TABLE I. Relaxed and unrelaxed vacancy formation energies for the various Cr magnetic structures. Values from other DFT studies are also shown for comparison: The energies from Ref. 9 are relaxed at constant volume, while the energy from Ref. 11 is relaxed with constant pressure. All the energies are in eV. Available experimental values are $H^f_{\mathrm{Vac}} = 2.00$ and 2.27 eV for $T \geqslant T_{\mathrm{Néel}}$ (Refs. 21,22).

			SDW		
E^f_{Vac}	AF	NM	Node	μ_{int}	μ_{max}
Unrelaxed	2.48	2.43	2.19	2.20	2.46
Relaxed	2.41	2.32	2.09	2.10	2.38
Other works	2.60[a]–2.71[b]	2.61[b]			

[a]Reference 11.
[b]Reference 9.

migration, and microstructural evolution of the materials. For $T \geqslant T_{\mathrm{Néel}}$, the formation and migration enthalpies derived from PAS data are respectively 2.00 eV $\leqslant H^f_{\mathrm{Vac}} \leqslant$ 2.27 eV and 0.95 eV $\leqslant H^m_{\mathrm{Vac}} \leqslant$ 1.25 eV.[21,22] For lower temperatures ($T \leqslant T_{\mathrm{Néel}}$), where accurate data may not be easily obtained by experiments, DFT calculations provide an alternative way.

Concerning the energetics, Table I shows both relaxed and unrelaxed vacancy formation energies for the various local magnetic environments considered, calculated as follows:

$$E^f_{\mathrm{Vac}} = E\big((n-1)\mathrm{Cr},\mathrm{Vac}\big) - \frac{n-1}{n}E(n\mathrm{Cr}), \qquad (1)$$

where $E\big((n-1)\mathrm{Cr},\mathrm{Vac}\big)$ and $E(n\mathrm{Cr})$ denote the total energies of an n-atom bcc Cr supercell with the same magnetic state, with and without a vacancy, respectively.

The resulting relaxed formation energies for the μ_{max} site and for the AF phase are 2.38 and 2.41 eV, respectively. These values are indeed degenerate. It is not surprising since both vacancy sites have similar magnetic environments. Indeed, the high-spin domain in the SDW state is around $5a_0$ wide with almost constant local moments ($\Delta\mu \leqslant 2\%$). On the other hand, fully relaxed vacancy formation energy in the NM Cr, 2.32 eV, is lower than in the AF phase. It is particularly interesting to note that the formation energies for a vacancy located at a node and at a μ_{int} site of SDW are both around 0.2 eV lower than in NM Cr. The preferential formation sites for a vacancy in the SDW state are therefore around a low-spin site.

When comparing both relaxed and unrelaxed formation energies (Table I), it can be noticed that relaxation effects are weak (around 0.1 eV) and seem to play a minor role on the relative stabilities of vacancies between the various SDW sites and the AF and NM phases. For instance, the node and the μ_{int} sites in the SDW state already have the lowest energies before relaxation. As expected for bcc metals, the first-neighboring atoms of a vacancy relax toward the vacancy in all the cases.[10] The relaxation amplitudes are around 1.0% of Cr-Cr first-neighbor distance for μ_{max} sites, and 1.7% at the low-spin sites.

The above energetic comparison suggests that considering vacancies in neither the simplified AF nor the NM structures may give reliable descriptions for the ground state of Cr, where an explicit representation of the SDW structure happens to be required.

The obtained results also reveal that the variation of vacancy formation energy is not strictly monotonously linked to the amplitude of the on-site local magnetic moment; e.g., the energy in NM Cr is higher than that at a node or a μ_{int} site of the SDW state. Thus, in order to understand how and how much vacancy and magnetic structure can influence each other, we plot in Fig. 2 the difference of magnetization between situations with and without a vacancy ($\Delta\mu$). These maps show the projection of two adjacent atomic layers including the vacancy on a (100) plane with either three parallel SDWs or layered AF patterns in an equivalent cell. Note that the (010) view (not shown) parallel to the wave vectors provides the same information, whereas the transversal (001) plane contains the vacancy and its 4 second neighbors and 4 third neighbors. We first note that magnetization around a vacancy is enhanced when it is located at all the three sites of SDW (node, μ_{int}, μ_{max}), as well as in the AF phase. The respective increase of local moments on first-neighbor atoms are up to 0.38, 0.79, 0.25, and 0.25 μ_B, respectively. Such increase is however much smaller in the phase where initial local moments of Cr atoms are zero; i.e., the vacancy only induces local moments of 0.10 μ_B on nearest-neighbor atoms. The local moment enhancement for low-spin sites (node and μ_{int}) is stronger than that for a high-spin site. The former comes to be particularly sensitive magnetically to the presence of vacancy. It is worth mentioning that when the vacancy is located at a μ_{int} site, not only the magnetic node of the SDW containing the defect is shifted toward the vacancy position, but also all the other eight neighboring waves within our simulation cell become asymmetric in a similar way, causing major magnetic perturbations as shown in Fig. 2(b).

Another difference between magnetic modifications induced by the presence of vacancy in SDW and the layered AF phase concerns anisotropic $\Delta\mu$ distribution in the former. Indeed, the range of magnetic perturbations may be longer along the SDW than perpendicular to it. For instance, this anisotropy can be noted in the case of a vacancy at a μ_{max} site [Fig. 2(a)]. We find a $\Delta\mu$ of -0.2 and $+0.2$ μ_B around its nearest-neighbor nodes, located at $5a_0$ away from the vacancy. These variations are also present at neighboring node sites belonging to other SDWs in the same simulation cell, which are more than $5a_0$ away from the vacancy. As expected, this magnetic anisotropy also induces a relaxation anisotropy of atoms which mainly move along directions parallel to the SDWs rather than perpendicular to them. Again, the magnetic variations induced by vacancy reveal key differences between simple AF and NM structures and SDW, where the impact of vacancy is stronger and longer ranged on the latter from a magnetic point of view.

To gain more insight into the vacancy formation in SDW-Cr, we have investigated the related changes of electronic structures. We plot in Figs. 3 and 4 the projected density of states (PDOS) on atoms surrounding the vacancy. We focus our discussion on the μ_{max} and node sites as the PDOS on atoms near a μ_{int} site appears to be very similar to that of a node site.

We observe a significant change of the electronic structure on the first neighbors of the vacancy induced by the vacancy: for both magnetic sites, an almost rigid shift of both majority and minority bands toward higher energies. We also observe an

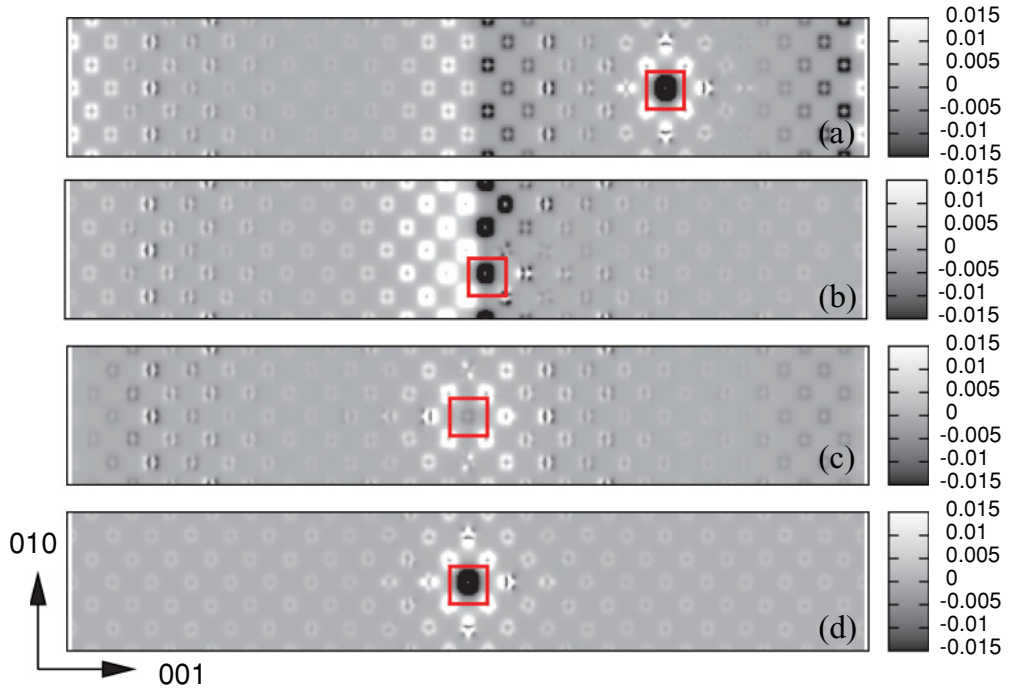

FIG. 2. (Color online) Difference of magnetization (in μ_B/a.u.^{3}) of Cr atoms with and without a vacancy located (a) at a $\mu_{\max}$ site of SDW, (b) at a μ_{int} site of SDW, (c) at a node of SDW, and (d) in AF Cr. Horizontal [001] and vertical [010] dimensions are respectively $20a_0$ and $3a_0$ long, where three SDWs are oriented along the [001] axis. The vacancy sites are pointed out with red (dark gray) empty squares.

increase of the PDOS of d character just before Fermi energy (E_F), which is stronger for the majority band. In addition to this shift, there is also a charge transfer from minority to majority bands, consistent with the local magnetic moment enhancement mentioned previously. However, the charge gain on Cr first neighbors of the vacancy is rather small ($+0.1\ e^-$) and independent of the vacancy site. At variance, for the farther neighbors of the $\mu_{\max}$-site vacancy, where a 0.2 μ_B of local moment change occurs, the only change of PDOS consists of an "on-site" transfer between up- and down-spin electrons, without any peak shift.

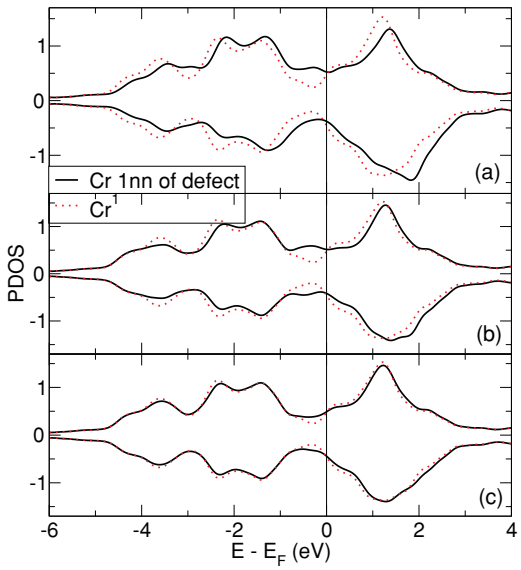

FIG. 3. (Color online) Projected density of states (PDOS) on first (1nn) Cr neighbors of (a) a vacancy, (b) a Cu atom, and (c) a Fe atom at a SDW node, compared with the PDOS of corresponding atom (Cr^1) in defect-free SDW Cr. Note that an average of the PDOS on two nonequivalent first neighbors of Fe is shown in (c). See Sec. III C for more details.

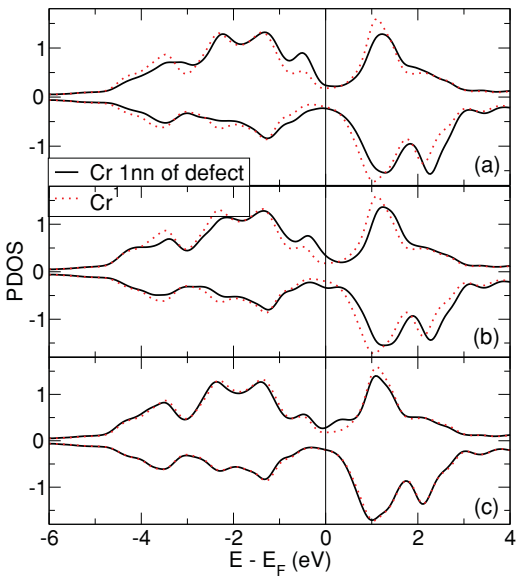

FIG. 4. (Color online) Projected density of states (PDOS) on first (1nn) Cr neighbors of (a) a vacancy, (b) a Cu atom, and (c) a Fe atom at a SDW-$\mu_{\max}$ site, compared with the PDOS of corresponding atom (Cr^1) in defect-free SDW Cr.

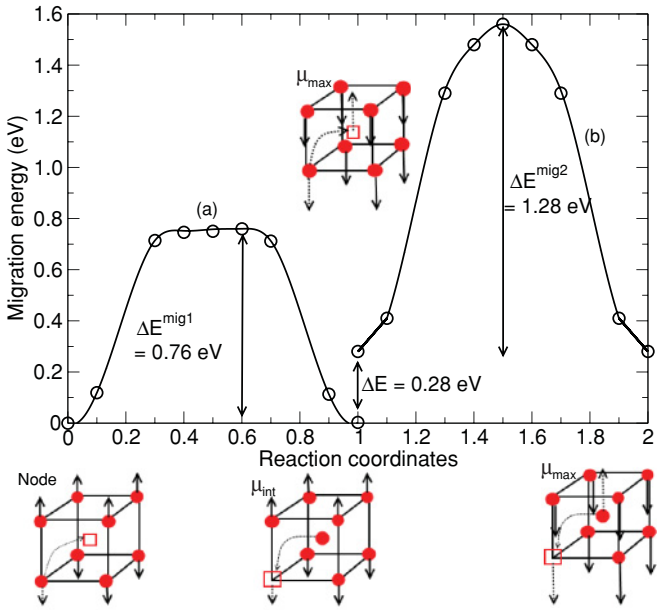

FIG. 5. (Color online) Migration barriers of vacancy between (a) node and $\mu_{\rm int}$ sites of SDW and (b) first-neighbor $\mu_{\rm max}$ sites of SDW. All the energies are in eV. Schematic views of initial and final metastable states with the corresponding vacancy displacements are also shown, where amplitudes of the local magnetic moments are proportional to the arrow lengths. Cr atoms are represented by red (dark gray) filled circles and vacancy by red (dark gray) empty squares.

In order to check the accuracy of the obtained energetic values, we have compared the calculated formation energies for the AF and NM to those from a previous DFT study[9] (Table I). The discrepancies of formation energies are around 0.3 eV (12%), which remains reasonable. Moreover, thanks to compensation of systematic errors, the difference of formation energies between the AF and NM phases are quantitatively the same between both DFT works. This comparison confirms the validity of the above main energetic discussions, i.e., the relative stability of vacancies at different magnetic sites.

B. Vacancy migration in SDW Cr

We have also investigated low-energy migration paths of vacancy in a SDW state by calculating energy barriers for jumps between neighboring sites. Figure 5 shows the barrier between a node and its nearest-neighbor $\mu_{\rm int}$ sites and that between two $\mu_{\rm max}$ sites. The obtained migration energy for the former is 0.76 eV. This jump is found to require a significantly lower barrier than that between neighboring $\mu_{\rm max}$ sites (1.28 eV). At variance with the formation energies, migration barriers for both node and $\mu_{\rm max}$ sites are essentially the same as in the NM and AF phases, respectively (0.82 and 1.32 eV). The amplitudes of local magnetic moments on the migrating Cr at the saddle point are respectively 0.77, 0.49, and 0.30 μ_B for the node and $\mu_{\rm max}$ sites and in the AF phase. The strong reduction of local moments in the latter two cases suggests the presence of magnetic frustration linked to the local magnetic environment of the migrating Cr. Indeed, the migrating Cr has six nearest neighbors at the saddle point, which show local moments of 1.23 and 1.28 μ_B, respectively, for the $\mu_{\rm max}$ site of SDW and the AF phase. The migrating Cr couples antiferromagnetically with only half of them, but ferromagnetically with the remaining three neighbors. At variance, near a node of SDW, the migrating Cr is ferromagnetically coupled with only two of its neighbors presenting lower local moments (0.83 μ_B), and antiferromagnetically with four of them (0.42 to 0.51 μ_B). The different distributions of local magnetic moments on nearest neighbors are qualitatively consistent with the difference of energy barriers found.

Experimentally, vacancy migration energies of various bcc transition metals, e.g., Fe, Mo, V, and W, have been accurately determined by isochronal resistivity recovery experiments after low-temperature electron irradiation.[21] However, very little is known about Cr. The most direct measurement comes from a weak increase of average positron lifetime in PAS studies, indicating that vacancies in Cr may migrate in order to agglomerate at 350 K, with a corresponding effective energy barrier of 0.95 eV.[21,22] It is worth mentioning that our calculated values suggest a strong migration anisotropy; i.e., the diffusion of vacancies in the SDW state ($T \lesssim 311$ K) is expected to be mainly confined within atomic planes perpendicular to the SDW direction, which contain the nodes and their first-neighbor sites (Fig. 5). This theoretical prediction indeed requires additional experimental confirmation, such as the very accurate resistivity recovery experiments as performed in high-purity Fe.[25,28] Also, more experimental vacancy migration data, including the predicted anisotropy, may be obtained when the temperature domain of SDW existence could be extended thanks to doping, for instance with Mn or Re.[13]

C. Properties of 3*d* substitutional impurities: Fe and Cu

The aim of this section is to investigate the properties of two representative 3*d* substitutional impurities and their possible impact on the magnetic structure of SDW. We have chosen Fe, a strongly magnetic element in the bcc lattice, and Cu, taken as a prototype of NM defect with full 3*d* band. These two elements present very small size difference with Cr in a bcc lattice. The respective calculated and experimental equilibrium atomic volumes are listed in Table II.

Similarly to the previous section, we show in Table III relaxed and unrelaxed solution energies of these substitutional impurities in Cr for various magnetic environments at very dilute concentration (0.27%), where the SDW state remains

TABLE II. Calculated and experimental equilibrium atomic volumes (in Å^3) are given for bcc Cr, Fe, and Cu, where the corresponding magnetic structures are indicated in parentheses. The experimental values have been measured at room temperature.

	This Study	Exp. (Ref. 21)
Cr	11.83(SDW)	11.97
	11.93(AF)	
	11.60(NM)	
Fe	11.80(FM)	11.80
Cu	12.33(NM)	

TABLE III. Relaxed and unrelaxed Fe and Cu solution energies for the various Cr magnetic structures considered. All the energies are in eV. A low-spin solution of higher relaxed energy ($E_{\mathrm{Fe}}^{\mathrm{sol}} = 0.46$ eV) exists for Fe at a SDW-node site.

			SDW		
E_X^{sol}	AF	NM	Node	μ_{int}	μ_{max}
Unrelaxed Fe	0.40	0.42	0.40	0.35	0.44
Relaxed Fe	0.38	0.29	0.27	0.28	0.39
Other works Fe	0.48[a]				
Unrelaxed Cu	1.44	1.40	1.22	1.12	1.47
Relaxed Cu	1.15	1.11	0.89	0.94	1.15

[a]Reference 11.

in each case the experimental ground state. The respective Fe and Cu solution energies are defined as

$$E_X^{\mathrm{sol}} = E\big((n-1)\mathrm{Cr}, X\big) - \frac{n-1}{n} E(n\mathrm{Cr}) - E(X), \quad (2)$$

where X = Fe or Cu. $E\big((n-1)\mathrm{Cr}, X\big)$ and $E(n\mathrm{Cr})$ denote the total energies of an n-atom bcc Cr supercell at the same magnetic state, with and without the impurity X, and $E(X)$ is the total energy per atom of either bcc FM Fe or NM Cu.

Concerning Cu, the obtained fully relaxed solution energies for all magnetic phases are positive, ranging from 0.89 to 1.15 eV, which is consistent with the known fact that the CrCu system is rather immiscible.[29] The difference of relaxed solution energies between the various sites follows a similar trend as the relaxed formation energies of a vacancy. Indeed, Cu at the μ_{max} site and in an AF phase shows the highest relaxed solution energies (1.15 eV), closely followed by the NM phase (1.11 eV), then the μ_{int} site (0.94 eV), and finally the node being the lowest in energy (0.89 eV). Moreover, in a SDW state, the energy differences between the μ_{max} and node sites are also similar for the dissolution of Cu and the formation of a vacancy: 0.26 and 0.29 eV, respectively. There are however some quantitatively different behaviors between both Cu and vacancy. For instance, Cu solution energies for the AF and the NM phases are much closer to each other, their difference (0.04 eV) being within the precision error bar of the present DFT calculations (0.05 eV).

The structural relaxation effects, estimated from the comparison between relaxed and unrelaxed energies, are qualitatively similar to what happens to the vacancy. Indeed, sites of weak magnetic environment are the lowest energy sites with and without relaxation. We nevertheless note an inversion between node and μ_{int} sites before and after relaxation. Besides, the energy variation due to relaxation is larger with Cu (around 0.3 eV) than with vacancy (0.1 eV). As expected, first-neighboring atoms of Cu show outward relaxations due to a larger atomic volume compared with Cr. The corresponding relaxation amplitudes in all the considered magnetic environments are about 2.5% of first-neighbor Cr-Cr distances.

The magnetic variation around Cu presented in Fig. 6 confirms its similar magnetic impact compared with the vacancy, i.e., increasing local moments of neighboring Cr atoms. We also observe for Cu a strong variation of μ on its nearest Cr neighbors when located at a μ_{int} site, which induces a node shift for its own and neighboring SDWs, creating a magnetic asymmetrization as in the vacancy case [Fig. 6(a)]. However, some minor differences exist between Cu and vacancy, which suggests a weaker effect of Cu on the magnetic structure of SDW. For instance, the local moment enhancement $\Delta\mu$ around Cu at the node ($0.22\,\mu_B$) is slightly smaller than around a vacancy at the same site ($0.38\,\mu_B$). Also, the long-range magnetic perturbation observed with vacancy at a μ_{max} site of SDW disappears with Cu.

From an electronic structure viewpoint, we note in Figs. 3 and 4, showing the PDOS on nearest Cr neighbors, that similar electron transfer toward high energies as in the vacancy case occurs. This causes an increase of PDOS just before Fermi level with the presence of a pick in both majority and minority states. The PDOS on Cu, in Fig. 7, shows an almost rigid band translation from around -2.1 eV to -4.0 eV which may be due to repulsion between the full $3d$ band of Cu with that of Cr. We also notice in the PDOS of Cu an increase of electronic states near the E_F, which may be attributed to a very slight hybridization of $3d$ Cu band with Cr. We moreover find a $0.23\,e^-$ charge transfer toward the Cu atom for all the magnetic environments in agreement with the higher electronegativity of Cu compared to Cr.

Concerning Fe, the obtained relaxed solution energies for the various Cr phases are all positive, which is in agreement with the phase separation tendency in CrFe alloys with low Fe content, as pointed out by recent DFT calculations.[11,30,31] However, the values are much smaller than for Cu, indicating a weaker unmixing tendency with Cr. Comparing various magnetic sites in Cr, relaxed solution energies of the μ_{max} site and AF state are the highest (0.39 and 0.38 eV, respectively), but not far from the NM state, the μ_{int}, and node sites, which all have the same energy (from 0.27 to 0.29 eV) within the estimated error bar of the present calculations. As we can see, in a SDW state, the energy difference between the μ_{max} and the node sites for Fe is lower than for Cu: 0.12 and 0.26 eV, respectively. We would like to mention that despite the smaller energy difference (0.12 eV), the predicted anisotropy of Fe solution sites in the SDW-Cr still seems to be in disagreement with the previous phenomenological model result, suggesting a random distribution of Fe atoms.[16]

The difference between relaxed and unrelaxed energies is very small, namely $\leqslant 0.05$ eV, when Fe is located at a μ_{max} site of SDW or in AF Cr, and 0.07 eV at a μ_{int} site. This is due to both a tiny size difference between Fe and Cr and small magnetic perturbation induced by Fe at those sites. In contrast, we note higher relaxation effects, around 0.12 eV for NM Cr and the SDW node, where the Fe atom adopts larger local moment. It also introduces stronger magnetic modification on surrounding Cr atoms in the latter case.

This reduction of energy difference between the various magnetic environments is actually due to the additional magnetic flexibility of the magnetic impurity. The magnetic modifications of SDW as plotted in Fig. 6 show clear differences between the Fe and Cu cases. Indeed, isolated Fe in Cr shows two alternative magnetic states: a high-moment state ($\mu \gtrsim 2\,\mu_B$) and a low-moment state (almost 0 μ_B). For the AF phase, the only energy minimum consists of a low-moment Fe. In view of previous results, we also expect

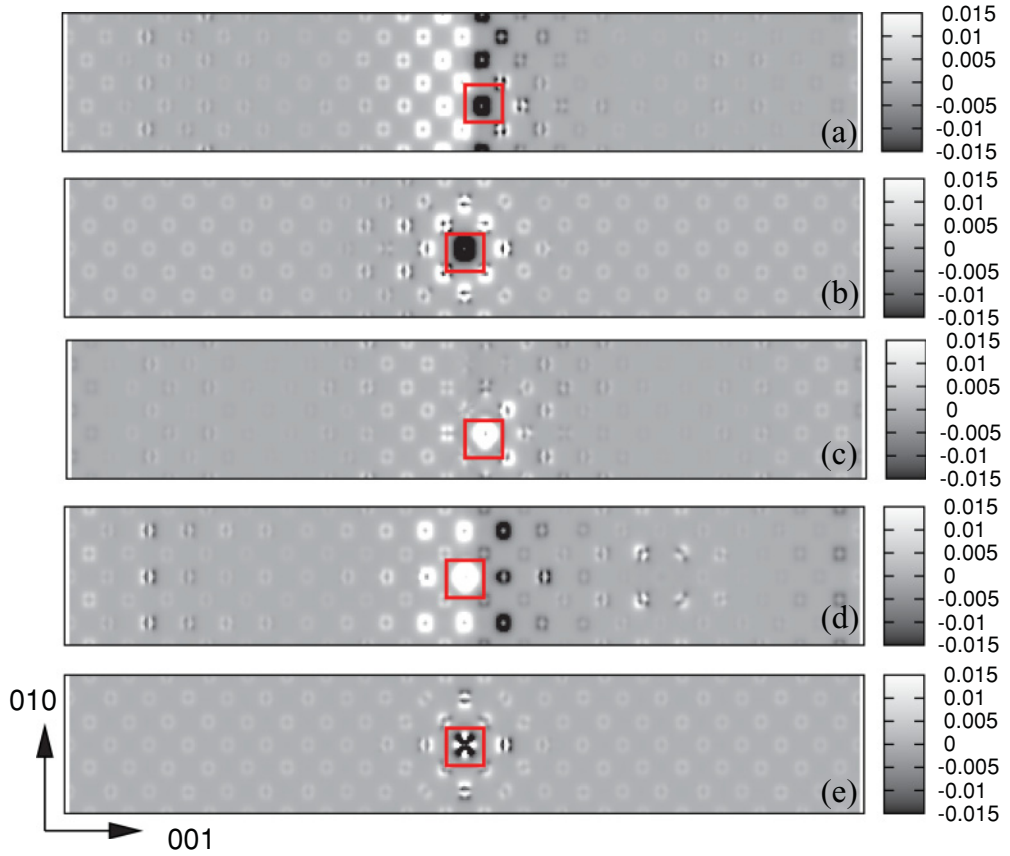

FIG. 6. (Color online) Difference of magnetization (in μ_B/a.u.^{3}) of Cr atoms with or without impurity: (a) Cu at a μ_{int} site of SDW, (b) Cu in AF Cr, (c) Fe at a μ_{int} site of SDW, (d) Fe at a node of SDW, (e) Fe in AF Cr. Horizontal [001] and vertical [010] dimensions are respectively $20a_0$ and $3a_0$ long, where three SDWs are oriented along the [001] axis. The impurity sites are pointed out with red (dark gray) empty squares.

a similar behavior for the μ_{max} site of SDW. This result is consistent with previous theoretical studies[30,32] predicting both first and second FeCr neighbors to prefer antiparallel magnetic coupling. Fe may therefore suffer from a magnetic frustration when located at those sites where neighboring Cr atoms show antiferromagnetic arrangements with strong moments. The

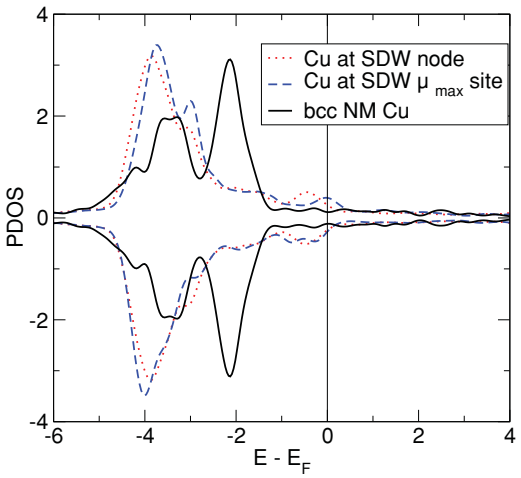

FIG. 7. (Color online) PDOS on a Cu atom embedded in SDW Cr compared to that of pure Cu in the bcc NM phase.

associated magnetic modification is similar to those induced by Cu, consisting of local increase of magnetization around the impurity. Nevertheless, such increase is much weaker than for Cu, only 0.04 μ_B on the nearest neighbors.

At variance, Fe adopts the high-moment state (1.88 μ_B) when embedded in NM Cr. When located at a node of SDW, Fe can be at either a low- or a high-moment state (2.09 μ_B), the latter being lower in energy with a ΔE of 0.18 eV. This high-moment state of Fe at a SDW node shows an unexpected magnetic configuration [Fig. 10(a)]. The presence of a high-moment Fe induces first of all a shift of SDW node toward its first-neighbor site, inducing thus asymmetrization of not only the SDW containing the Fe atom, but also the neighboring SDWs. This asymmetry is reflected in the strongly disturbed magnetic structure shown in Fig. 6(d), where we note an increase of magnetization on the left side of Fe and a decrease on the right side where new nodes are created. In addition to that, Fe is coupled ferromagnetically with one-half of the Cr first neighbors of rather high local moments ($\mu = 1.00\,\mu_B$). The remaining half of Cr nearest neighbors, which are NM, determine the shifted new nodal plane. On the other hand, the Fe is coupled antiferromagnetically with 5 of the 6 Cr second-nearest neighbors, showing significant local moments, ranging from 0.42 to 1.15 μ_B. This complex magnetic structure may also result from the interplay between various coupling tendencies, e.g., the suggested antiparallel

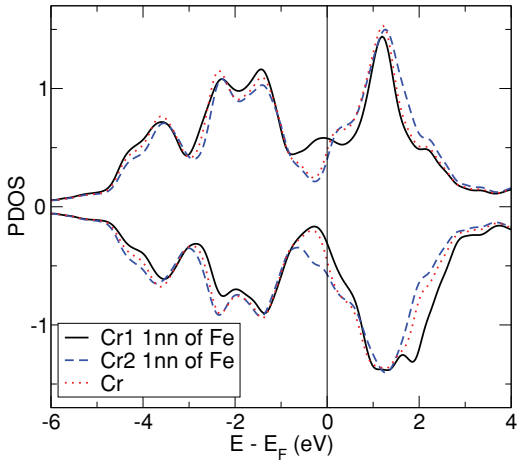

FIG. 8. (Color online) PDOS on first-nearest Cr neighbors of Fe at a SDW node compared with the PDOS of the corresponding atom in pure SDW Cr. The 2 first-nearest Cr neighbors become nonequivalent in the presence of Fe: Cr1 with an increased magnetic moment and Cr2 being a new node site.

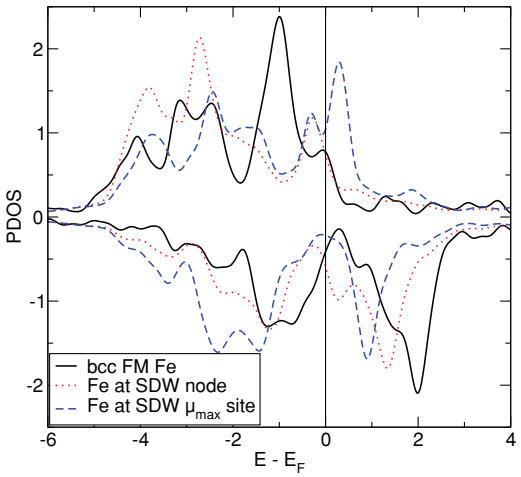

FIG. 9. (Color online) PDOS on a Fe atom embedded in SDW-Cr compared to that of pure Fe in the bcc FM phase.

coupling tendency of Fe with both first- and second-neighbor Cr atoms.

For an intermediate case, Fe being at a μ_{int} site, its resulting local moment is 2.00 μ_B. We note that the nearest-neighbor Cr atoms have the same local moments as for Cr atoms around Fe at a node [Fig. 10(a)]. However, in the absence of magnetic node shift, the SDWs remain symmetric in the μ_{int} case.

From the electronic structure point of view, we note in Fig. 4 that the PDOS on Cr neighbors are indeed less sensitive to the presence of Fe than Cu or vacancy at a μ_{max} site of SDW. When Fe is at a node of SDW, Fig. 8 reveals that, consistent with the magnetic modifications, the two Cr first neighbors of the same SDW become inequivalent due to node shift. We observe for Cr1, of large magnetic moment, an electron transfer from minority to majority band and a stronger PDOS increase just before E_F in the majority band. At variance, we observe for Cr2, of zero local moment, a transfer from majority to minority band and a strong PDOS increase about E_F in minority spin band. We however notice from Fig. 3(c), which shows the averaged PDOS of Cr1 and Cr2, that modification of the PDOS on Cr first neighbors is only minor.

In fact, all the electronic structure changes are focused on the Fe atom with a charge gain of around $+0.3\ e^-$ at all the magnetic sites considered. For the high-moment Fe located at the node of SDW, there is a strong electron transfer in majority states from high-energy pick of pure Fe at -1.0 eV to lower energy picks (from -2 to -4 eV) (Fig. 9). For low-moment Fe located at a μ_{max} site of SDW, the influence of surrounding Cr atoms is even larger, where both majority and minority bands show strong hybridization with Cr atoms, as suggested by the previous study based on magnetic susceptibility measurements.[16]

D. Properties of an Fe dimer in Cr

We also compared the magnetic and energetic properties of a Fe dimer embedded in Cr with various magnetic environments. We focused on situations where the two Fe atoms are first-nearest neighbors, which give clues concerning segregation tendency of Fe in Cr.

Local magnetic moments of the Fe dimer in AF and NM Cr as well as at a SDW node are shown in Table IV. Note that in the latter case, one of the Fe atoms is located at the node and the other at the neighboring μ_{int} site. Also, as expected, the dimer at a μ_{max} site behaves in a similar way as in AF Cr.

Local energy minima with different magnetic arrangements may exist when a nearest-neighbor Fe dimer is included in Cr. For instance, two different configurations are found for AF Cr (and the μ_{max} site of SDW) within the present collinear approximation. A high-energy state consists of both Fe atoms presenting negligible local moments. This is indeed due to magnetic frustration resulting from competition between different magnetic coupling tendencies. As with one Fe in AF Cr, Fe-Cr first and second neighbors and Cr-Cr first neighbors all prefer antiparallel coupling. In addition, the two Fe atoms tend to have parallel local moments. Another state, 0.03 eV lower in energy, consists of one high-moment (2.26 μ_B) and another low-moment Fe (0.67 μ_B). This asymmetric structure may allow the partial release of the magnetic frustration of the Fe atoms. In order to gain more insight into the magnetic frustration, we have performed a complementary calculation by relaxing the collinear constraint. As a result, a third magnetic configuration is found where the local moments of the two Fe atoms, parallel to each other, are orthogonal to the Cr atoms. The Fe atoms show the same intermediate moments of 1.87 μ_B each. This result suggests that the magnetic frustration

TABLE IV. Binding energies (in eV) between two nearest-neighbor Fe atoms for various Cr magnetic structures, where a positive value indicates an attractive interaction. Two values for the AF state refer to two different collinear magnetic arrangements as shown by the respective Fe local moments (in μ_B).

Cr Environment	AF	AF	NM	SDW Node
E^b(Fe-Fe)	−0.01	−0.04	0.15	0.12
μ_{Fe1}	2.26	0.07	1.95	2.06
μ_{Fe2}	0.67	0.06	1.95	2.04

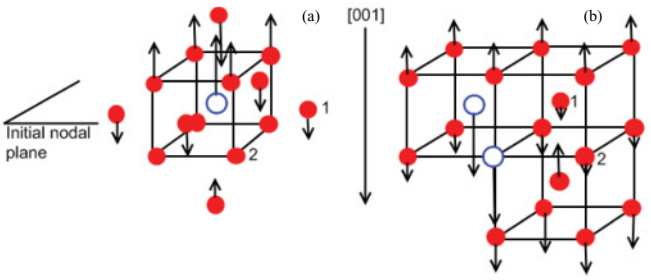

FIG. 10. (Color online) Schematic representation of magnetic structures of (a) an isolated Fe and (b) a Fe dimer at a node of SDW, where amplitude of each local magnetic moment is proportional to the arrow lengths. The Cr atoms are represented by red (dark gray) filled circles and the Fe atoms by blue (dark gray) empty circles. (a) After Fe insertion, the node of SDW is shifted from position 1 to position 2. As a result, Fe is coupled ferromagnetically with 4 Cr first-nearest neighbors and antiferromagnetically with 5 of the 6 Cr second-nearest neighbors. (b) With a Fe dimer, a small magnetic moment is induced on the original node site (position 1) while the magnetic moment on position 2 is decreased.

may also be partly relaxed by a non-collinear arrangement. In terms of energy, this configuration is slightly below (0.04 eV) the asymmetric collinear state mentioned above.

On the other hand, Fe dimers surrounded by low-moment Cr atoms adopt a different magnetic arrangement. For instance, both Fe atoms are strongly magnetic and coupled ferromagnetically in NM Cr. They also present a similar magnetic state at the node and μ_{int} sites of SDW, in qualitative agreement with previous experimental evidence considering FeCr alloys with 1.5% and 2.7% of Fe.[16] Around the node site, the Fe dimer strongly modifies local magnetic moments of surrounding Cr atoms. As shown in Fig. 10(b), a small magnetic moment (0.38 μ_B) appears at the original node site (labeled 1), whereas the local moment of a first-nearest Cr neighbor atom (labeled 2) decreases from 0.54 to 0.34 μ_B. This magnetic evolution may be seen as a node migration of one-half of the Cr-Cr interatomic distance. Again, as for isolated Fe in Cr, this complex magnetic structure may result from the subtle interplay between various coupling tendencies, particularly the antiparallel coupling of Fe with both first- and second-neighbor Cr atoms together with the strong Fe-Fe parallel coupling.

The binding energies between the Fe atoms [E^b(Fe-Fe)] resulting from the magnetic configurations described above can be calculated as

$$E^b_{\text{Fe-Fe}} = -E\big((n-2)\text{Cr},2\text{Fe}\big) + 2E\big((n-1)\text{Cr},\text{Fe}\big) - E(n\text{Cr}), \quad (3)$$

where $E\big((n-2)\text{Cr},2\text{Fe}\big)$ and $E\big((n-1)\text{Cr},\text{Fe}\big)$ are the total energies of Cr systems containing respectively two first-neighbor Fe atoms and one isolated Fe, and $E(n\text{Cr})$ is the total energy of a perfect n-atom Cr bulk. All the systems, with and without Fe, have the same initial magnetic structure. The obtained values for the various collinear configurations are listed in Table IV, showing significant binding enhancement between Fe atoms when switching from AF to both NM phase and the node site of SDW. This result is indeed consistent with the energetically favorable high Fe moments and strong ferromagnetic coupling at the low-spin Cr environments.

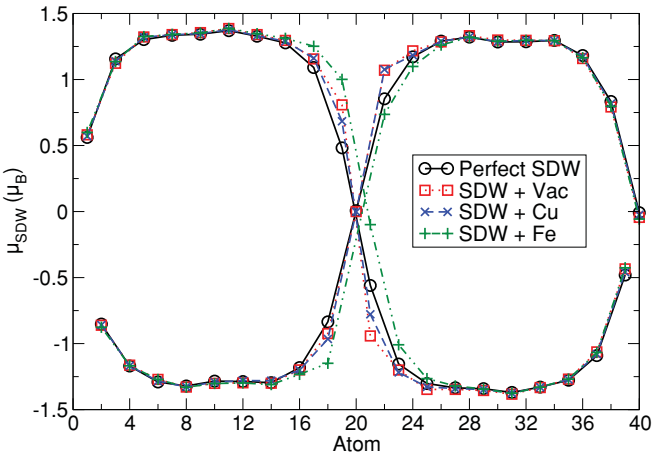

FIG. 11. (Color online) Profile of local magnetic moments of a SDW Cr with and without defect (Vac, Cu, and Fe), where the magnetic moments are given in μ_B.

Although the negative values in AF Cr may indicate small repulsion between Fe atoms, they are essentially negligible comparing with our precision error bar (0.05 eV). The positive values of E^b(Fe-Fe) in NM Cr and at a node of SDW Cr show however clear attraction between Fe atoms which favors Fe clustering in Cr.

E. Effects of vacancy, Cu, and Fe on the SDW structure

After considering the energetic, magnetic, and electronic features of vacancy, Cu, and Fe in Cr, we attempt to compare the impacts of these point defects on the magnetic structure of SDWs.

Despite only few experimental data being available concerning the atomic-scale effect of those point defects on the stability of SDW Cr, we know from the previous study of Tsunoda[14] that SDW is stable at low temperatures with less than 1.6% of Fe. Our results also confirm that the overall shape of a SDW with very low concentrations of point defects ($\lesssim$0.55%) is preserved, even though its magnetic structure may be locally modified to adapt the inclusion of defect. Indeed, as illustrated in Fig. 11 for various defects located at the preferential site, i.e., the magnetic node, the SDW profiles become only slightly more rectangular due to local increase of Cr moments. However, no flip of Cr moment has been observed. As a consequence, the SDW is only getting closer to a limiting structure with two AF domains rotated 180° around the wave vector from each other, separated by a nodal plane. This structure is found to be unstable in pure Cr and tends to decay to the original SDW according to our DFT calculations.

Due to the limited simulation cell size and the applied periodic boundary conditions, the determination of the SDW-to-AF transition mechanism is beyond the scope of this study. Nevertheless, the present results may give some hints on the first step of defect-induced magnetic phase transition. For instance, when Fe is located at a node site of the initial SDW, the original node is shifted toward the first-neighbor site. Similarly, when a vacancy or Cu is located at a μ_{int} site, its nearest-neighbor node is naturally shifted to the defect site. Such node shifts occur not only in the SDW including the

defect, but also in neighboring waves. Such a node migration is indeed similar to the elementary mechanism pointed out by previous theoretical studies,[33,34] which has been proposed to be the first step toward node annihilation to explain a possible transition path from SDW to AF state. Point-defect insertion in SDW may therefore contribute to activate this local node migration mechanism.

IV. CONCLUSIONS

The aim of this study is to investigate the properties of the simplest structural defect (vacancy) and substitutional impurities (Fe, Cu) in the ground state of bcc Cr, i.e., the well-known SDW, by efficient DFT calculations with localized basis functions.

We first point out that although magnetic and energetic properties of these defects at the high-spin sites of SDWs are similar to those predicted in a simple AF phase, their lowest energy site is always around the node of a SDW, as compared with other SDW sites and the AF and the NM phases. The energy difference between the SDW node and $\mu_{\max}$ site ranges from 0.29 eV for a vacancy to 0.12 eV for Fe. Migration of vacancy is also favored around the SDW nodes, showing an anisotropic path, mainly confined in the nodal and adjacent planes. The obtained energy barriers are 0.76 eV around a node site, and 1.28 eV at the $\mu_{\max}$ site. Please note that besides the precision error (0.05 eV) of the present approach as described in Sec. II, the above-listed energies may also be quantitatively affected by the reversal of the relative stability between the SDW and the AF states, when comparing the DFT-GGA prediction with the experimental data. However, as the SDW state is only 0.014 eV per atom higher in energy than the AF state, we do not expect our energetic results (tenth of eV) to be significantly changed due to this error source.

The present results also strongly suggest that simple AF and NM phases may not allow an accurate description of defect properties in the ground state of Cr ($T \lesssim T_{\text{Néel}}$). Instead, an explicit SDW representation is required.

We have shown that vacancy and Cu both interact in a similar way with the Cr SDW. Indeed, relative stabilities of a vacancy and Cu in AF and NM phases and the various SDW sites are very close. Also, the electronic and magnetic modifications are essentially supported by neighboring Cr atoms, and there is no relevant role of structural relaxation on defect relative stabilities. The situation is however different with a strongly magnetic defect such as Fe. At variance with vacancy or Cu, energetic differences between the various magnetic sites are significantly smaller. The magnetic and electronic changes due to Fe addition are mainly supported by the impurity atom, which modifies its magnetic state depending on the magnetism of surrounding Cr atoms. The Fe electronic structure may also be strongly modified due to d-band hybridization with the Cr atoms. In this way, structural relaxations induced by Fe are found to be closely related to the magnetic perturbations on surrounding Cr atoms. They do play a relevant role in dictating relative stability of the different sites.

Concerning the impact of point defects on SDW structures, we find node shifts to first-nearest neighbor sites induced by the insertion of either a vacancy, Cu, or Fe around the SDW nodes. This node shift may contribute to promote node migration and annihilation, previously proposed as a possible transformation path from the SDW to the AF state.

ACKNOWLEDGMENTS

This work was performed using HPC ressources from GENCI-CINES (Grants No. 2010-x2010096020 and No. 2011-x2011096020).

[1] L. Corliss, J. Hastings, and R. Weiss, Phys. Rev. Lett. **3**, 211 (1959).
[2] V. Bykov, V. Golovkin, N. Ageev, V. Levdik, and S. Vinogradov, Dokl. Akad. Nauk SSSR **4**, 1149 (1958).
[3] E. Fawcett, Rev. Mod. Phys. **60**, 209 (1988).
[4] R. Hafner, D. Spisak, R. Lorenz, and J. Hafner, Phys. Rev. B **65**, 184432 (2002).
[5] S. Cottenier, B. De Vries, J. Meersschaut, and M. Rots, J. Phys. Condens. Matter **14**, 3275 (2002).
[6] V. L. Moruzzi and P. M. Marcus, Phys. Rev. B **42**, 8361 (1990).
[7] K. Hirai, J. Phys. Soc. Jpn. **66**, 560 (1997).
[8] R. Soulairol, C.-C. Fu, and C. Barreteau, J. Phys. Condens. Matter **22**, 295502 (2010).
[9] P. Olsson, C. Domain, and J. Wallenius, Phys. Rev. B **75**, 014110 (2007).
[10] P. Soderlind, L. H. Yang, J. A. Moriarty, and J. M. Wills, Phys. Rev. B **61**, 2579 (2000).
[11] K. O. E. Henriksson, J. Nucl. Mater. **395**, 45 (2009).
[12] P. Olsson, J. Nucl. Mater. **386**, 86 (2009).
[13] E. Fawcett, H. Alberts, V. Galkin, D. Noakes, and J. Yakhmi, Rev. Mod. Phys. **66**, 25 (1994).
[14] Y. Tsunoda, J. Phys. Condens. Matter **6**, 8513 (1994).
[15] V. Galkin, P. de Camargo, N. Ali, and E. Fawcett, J. Appl. Phys. **81**, 4207 (1997).
[16] V. Galkin, W. Ortiz, and R. Fishman, J. Magn. Magn. Mater. **186**, L1 (1998).
[17] R. S. Fishman and S. H. Liu, Phys. Rev. B **45**, 12306 (1992).
[18] V. M. Uzdin, H. Zabel, A. Remhof, and B. Hjorvarsson, Phys. Rev. B **80**, 174418 (2009).
[19] K. Hirai, Phys. Rev. B **59**, R6612 (1999).
[20] R. Fishman, J. Phys. Condens. Matter **13**, R235 (2001).
[21] Landolt-Börnstein, *Atomic Defects in Metals* (Springer Materials, Berlin, 1985).
[22] J. Campbell and C. Schulte, Appl. Phys. **19**, 149 (1979).
[23] J. Soler, E. Artacho, J. Gale, A. Garcia, J. Junquera, P. Ordejón, and D. Sanchez-Portal, J. Phys. Condens. Matter **14**, 2745 (2002).
[24] C. C. Fu, F. Willaime, and P. Ordejon, Phys. Rev. Lett. **92**, 175503 (2004).
[25] C. C. Fu, J. Dalla Torre, F. Willaime, J. L. Bocquet, and A. Barbu, Nature Mater. **4**, 68 (2005).

[26]F. Soisson and C.-C. Fu, Phys. Rev. B **76**, 214102 (2007).
[27]C. C. Fu and F. Willaime, Phys. Rev. B **72**, 064117 (2005).
[28]S. Takaki, J. Fuss, H. Kugler, U. Dedek, and H. Schultz, Radiat. Eff. **79**, 87 (1983).
[29]H. Okamoto, J. Phase Equilibria **22**, 691 (2001).
[30]T. P. C. Klaver, R. Drautz, and M. W. Finnis, Phys. Rev. B **74**, 094435 (2006).
[31]A. T. Paxton and M. W. Finnis, Phys. Rev. B **77**, 024428 (2008).
[32]M. Y. Lavrentiev, D. Nguyen-Manh, and S. L. Dudarev, Phys. Rev. B **81**, 184202 (2010).
[33]V. Vanhoof, M. Rots, and S. Cottenier, Phys. Rev. B **80**, 184420 (2009).
[34]V. Uzdin and C. Demangeat, J. Phys. Condens. Matter **18**, 2717 (2006).